CHARACTERISTICS OF PLANE JETS IN THE TRANSITION REGION

Il Won Seo[1], Jung Kyu Ahn[2], and Seok Jae Kwon[3]

[1] Prof., Dept. of Civil Engineering, Seoul National Univ., Seoul, Korea
[2] Grad. Student, Dept. of Civil Engineering, Seoul National Univ., Seoul, Korea
[3] Grad. Student, Dept. of Civil Engineering, Seoul National Univ., Seoul, Korea

Abstract: In this study, laboratory experiments have been performed to investigate characteristics of the velocity fields and turbulence for non-buoyant plane jet in the vicinity of the jet nozzle using PIV system. The experimental results show that, in the transition region, the lateral velocity profile is in good agreement with Gaussian distribution. However, the coefficient of Gaussian distribution, k_u, decreases with longitudinal distance in the transition region. The existing theoretical equation for the centerline velocity tends to overestimate the measured data in the transition region. A new equation for the centerline velocity derived by incorporating varying k_u gives better agreement with the measured data than the previous equation. The results of the turbulence characteristics show peak values are concentrated on the shear layers. The Reynolds shear stress profile shows the positive peak in the upper layer and negative peak in the lower layer. The turbulent kinetic energy also provides double peaks at the shear layers. The peak of the Reynolds shear stress and the turbulent kinetic energy increases until x/B=8, and then it decreases afterwards.

Key Words: two-dimensional plane jet, experiments, PIV, ZFE, ZEF, transition region

1. INTRODUCTION

The study of mechanics of a turbulent jet requires better understanding of the process of jet growing by entrainment of surrounding fluids. Amongst the various types of turbulent jets, a plane jet is a typical case of free turbulence flows, and is used in practical purposes in many engineering fields (Kim *et al.*, 2001). The previous experimental observations on the velocity field for the non-buoyant plane jet indicate that, in the axial direction of jet, flow region can be divided into two distinct zones: zone of flow establishment (ZFE) and zone of established flow (ZEF) as shown in the Fig. 1. The ZFE, close to the nozzle, is commonly known as the zone where the turbulence penetrates inwards toward the axis of the jet. In the ZFE, the potential core, the wedge-like region of undiminished mean velocity, exists and is surrounded by mixing layers (Rajaratnam, 1976). In the ZEF, the turbulence already penetrates all the way to the jet axis and, as a result, the potential core disappears. The ZEF can further be divided into two regions; transition region and self-preserving region. In the self-preserving region, the jet flow

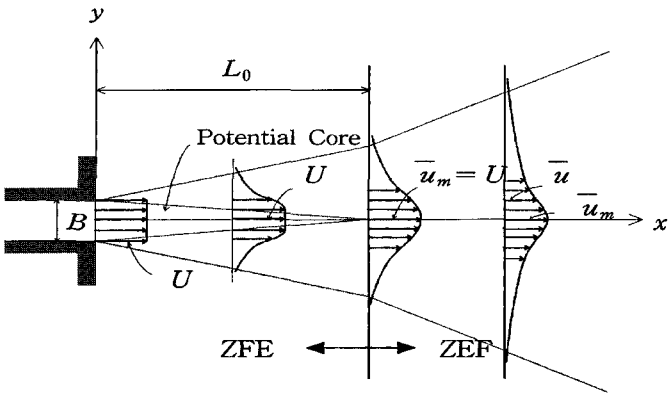

Fig. 1. Schematic Diagram of a Plane Jet

becomes self-similar. Therefore, most of the theoretical solutions for velocity and tracer concentration profile, trajectory and other values for the jet flow in ZEF were developed based on self-similarity assumptions.

Previous studies on the subject of turbulent jets, especially in environmental hydraulics, have mainly focused on the flow characteristics in the self-preserving region. Since the pioneering research by Morton *et al.* (1956), a considerable number of experimental, theoretical, and numerical investigations of turbulent jets in the self-preserving region have been performed (Crow and Champagne, 1971; Fischer *et al.*, 1979; Gutmark and Grinstein, 1999). Dilutions, trajectories, velocity distributions, turbulence characteristics and other topics of interest to environmental engineers are now well understood in this region.

The present paper describes some results of a series of laboratory experiments for the mechanics of two-dimensional non-buoyant plane jet in the ZFE and transition region. The mean velocity fields along with the turbulent characteristics were measured in depth using particle image velocimetry. A comparison between the results of the present study and theoretical equations has also been made in an attempt to understand the behavior of jet flows in more detail.

2. RESEARCH BACKGROUNDS

2.1 Plane Jet

The schematic diagram of the two-dimensional jet issuing from a slot is shown in Fig. 1. In this figure, B is the height of the slot and L_0 is the length of potential core, in which the velocity of the jet axis U remains constant. The outer lines represent the jet nominal boundaries where the horizontal velocity $\bar{u}$ is some arbitrarily small fraction of the centerline velocity. For values of x greater than L_0, the centerline velocity $\bar{u}_m$ is less than U.

Early semiempirical researches based on the assumption of geometrical similarity of velocity profiles in the self-preserving region of the jet have been developed(Daily and Harleman, 1966; Lozanova and Stankov, 1998). The similarity condition implies that

$$\bar{u}/\bar{u}_m = f(\xi) \tag{1}$$

where $\xi = y/x$.

Assuming that the velocity profile can be approximated by Gaussian curves, the following development for the plane jet can be illustrated as

$$\bar{u}/\bar{u}_m = f(\xi) = \exp\left[-k_u(y/x)^2\right] \tag{2}$$

where k_u is an experimental coefficient. The condition of constant momentum flux for two-imensional jets can be described as (Daily and Harleman, 1966)

$$\rho U^2 B = \rho(\bar{u}_m)^2 \int_{-\infty}^{\infty} f^2(\xi)\, dy \tag{3}$$

or

$$U^2 B = (\bar{u}_m)^2 x I_2 \tag{4}$$

where

$$I_2 = \int_{-\infty}^{\infty} f^2(\xi)\, dy \tag{5}$$

Therefore, the ratio of the centerline velocity to the initial jet velocity may be expressed in the following form.

$$\bar{u}_m/U = \sqrt{B/xI_2} \tag{6}$$

The length of the potential core, L_0, shown in Fig. 1, is derived using the condition of $\bar{u}_m/U = 1$ at $x = L_0$. Therefore, the length of potential core may be described as

$$L_0 = B/I_2 \tag{7}$$

Albertson *et al.* (1950) proposed that $I_2 = 0.192$. If this value is used, Eqs. (6) and (7) become

$$\bar{u}_m/U = 2.28\sqrt{B/x} \tag{8}$$

$$L_0 = 5.21B \tag{9}$$

2.2 Two-dimensionality of Flow Field

In this study, velocity profiles and turbulent characteristics are analyzed using the theory of two-dimensional jets, even though the rectangular nozzle used in this study has the aspect ratio, L/B, of 20 (L=100 mm; B=5 mm). Thus, the assumption of two dimensionality of the rectangular jet should be checked.

Fig. 2 shows the three-dimensional jet issued from the rectangular nozzle with finite length, L. In this study, the velocity fields were mearsured along z = 0. Therefore, the mixing phenomena in z-direction was not taken into account in this analysis. However, in reality, as the jet grows with x, the mixing in the z-direction will increase. Pani and Parameswaran (1994) developed the theoretical expressions representing the velocity profiles of the three-dimensional rectangular jet using the point source concept. In their approach, the solution for a point source was obtained using the momentum equation for an axially symmetric flow based on Reichardt's hypothesis. It was also assumed that the pressure contributed by the fluctuating componenet of flow, u', is an order of magnitude smaller than the mean dynamic quantity (Pani and Parameswaran, 1994).

In Fig. 2, for an elemental source of area, dA, the expression based on the point source concept can be expressed as

$$\frac{\bar{u}_m^{-2}}{U^2} = \frac{dA}{2\pi b^2} \tag{10}$$

where $b = cx$ and, c is an experimental coefficient. Each source of area "dA" contributes a certain dynamic pressure at the point "P". As the governing equation is linear, the principle of superposition can be adopted to find the resultant dynamic pressure at the point P. Hence, it

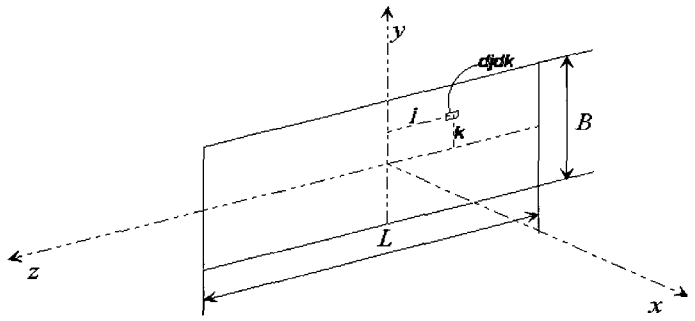

Fig. 2. Sketch of Three-Dimensional Rectangular Jet

can be given by

$$\frac{\bar{u}^2}{U^2}=\int_{-L/2}^{L/2}\int_{-B/2}^{B/2}\frac{1}{2\pi b^2}\exp\left[-\frac{1}{2}\left\{\left(\frac{z-j}{b}\right)^2+\left(\frac{y-k}{b}\right)^2\right\}\right]djdk \tag{11}$$

where $\bar{u}$ is the mean velocity at the point P in the x direction. Eq. (11) may be integrated to yield the final relationship as

$$\frac{\bar{u}^2}{U^2}=\frac{1}{4}\left\{erf\left(\frac{y-B/2}{\sqrt{2}b}\right)-erf\left(\frac{y+B/2}{\sqrt{2}b}\right)\right\}\left\{erf\left(\frac{z-L/2}{\sqrt{2}b}\right)-erf\left(\frac{z+L/2}{\sqrt{2}b}\right)\right\} \tag{12}$$

Along the longitudinal axis of the jet, $y=0$ and $z=0$. Thus, the centerline velocity distribution can be expressed as

$$\frac{\bar{u}_m^2}{U^2}=erf\left(\frac{B}{2\sqrt{2}b}\right)erf\left(\frac{L}{2\sqrt{2}b}\right) \tag{13}$$

For the two-dimensional jet, L can be assumed to be infinite. Therefore, Eqs. (12) and (13) can be converted into the following equations.

$$\frac{\bar{u}^2}{U^2}=-\frac{1}{2}\left\{erf\left(\frac{y-B/2}{\sqrt{2cx}}\right)-erf\left(\frac{y+B/2}{\sqrt{2cx}}\right)\right\} \tag{14}$$

$$\frac{\bar{u}_m^2}{U^2}=erf\left(\frac{B}{2\sqrt{2cx}}\right) \tag{15}$$

Comparing Eq. (15) with Eq. (8), the constant c can be obtained as 0.0778.

In this study, as mentioned above, the velocity measurements were done along z=0, and the aspect ratio is 20 (L=20B). Therefore, the substitution of z=0, L=20B, and c=0.0778 into (12) and (13) provides the centerline velocity profile for the rectangular jet used in this study as

$$\frac{\bar{u}^2}{U^2}=-\frac{1}{2}\left\{erf\left(\frac{y-B/2}{0.11x}\right)-erf\left(\frac{y+B/2}{0.11x}\right)\right\}\left\{erf\left(\frac{10B}{0.11x}\right)\right\} \tag{16}$$

$$\frac{\bar{u}_m^2}{U^2}=erf\left(4.455\frac{B}{x}\right)erf\left(90.91\frac{B}{x}\right) \tag{17}$$

The two-dimensional centerline velocity profiles can be derived from Eqs. (8) and (15) whereas the velocity profiles of three-dimensional rectangular jet used in this study can be obtained using Eq. (17). Fig. 3 shows the comparison between the centerline velocity decays of two and three-dimensional jets. It is noticed that the velocity profile for the two dimensional jet is in very good agreement with that for the three-dimensional jet for x/B<70. However, the centerline velocity of the three-dimensional jet decays faster than that of two-dimensional jet when x/B is greater than 70. This implies that the mixing in the z-direction may be negligible in the range of x/B<70 for the rectangular jets having the aspect ratio of 20 that

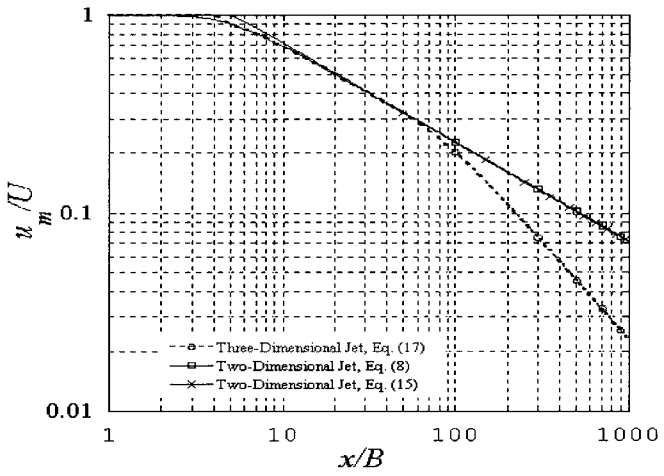

Fig. 3. Comparison of Two-Dimensional with Three-Dimensional Jets

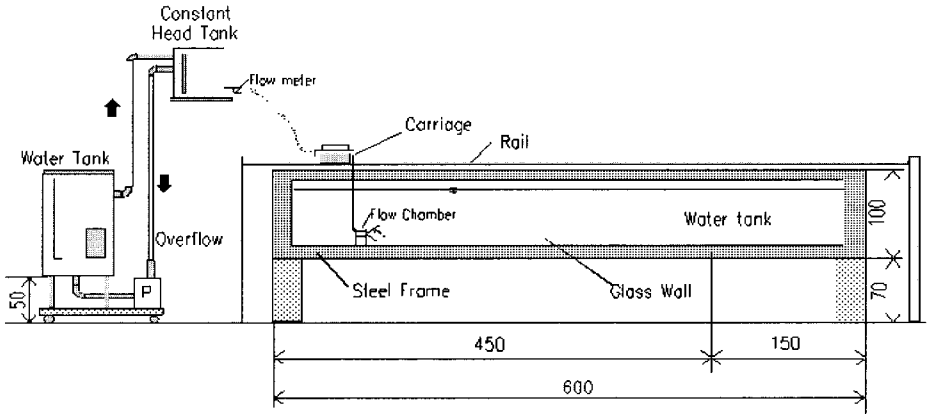

Fig. 4. Schematics of Experimental Tank for Near-Field Experiments (unit : cm)

is used in this study.

3. EXPERIMENTS

3.1 Experimental Apparatus and Measuring Equipment

The experiments have been carried out in a glass-walled rectangular tank that is 6.0 m long, 1.2 m wide, 1.0 m high as shown in Fig. 4. A constant head tank was used to ensure the constant outlet velocity of the jet. The experimental tank without a drainage system results in the increase of the volume of ambient water during the experiment. This might lead to the slight change of head difference (about 270 cm) between the constant head tank and water tank. However, in this study, the change of head difference, 0.23 – 0.68 mm/min., was assumed to be negligible since it was expected that the slight head difference did not have any influence on the jet behavior due to the short time (< 1

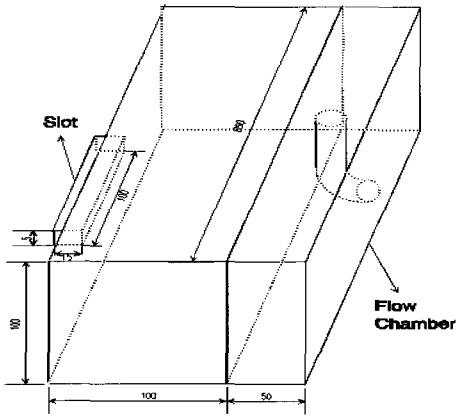

Fig. 5. Schematic of Flow Chamber and Slot (unit: mm)

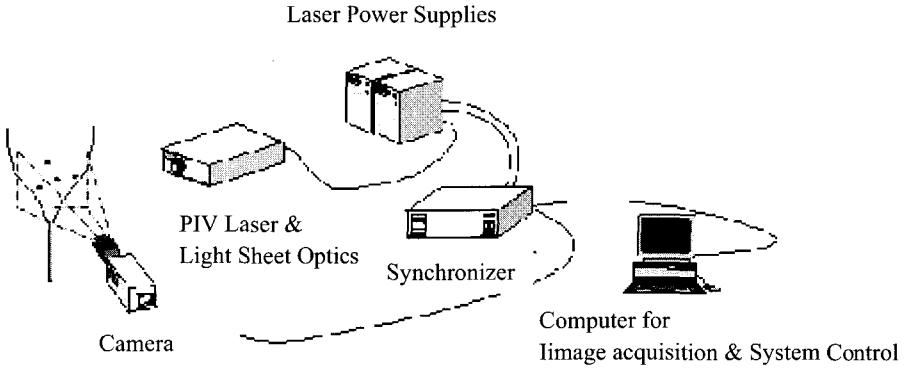

Fig. 6. Typical Setup for PIV System

min.) to capture the images .

The rectangular nozzle (slot) is attached at the side of the water chamber as shown in Fig. 5. This water chamber is placed on the proper distance (about 30 cm) from the bottom to avoid boundary attachment of the horizontally issuing jet. The slot consists of round-edged intake allowing the top hat distribution in the initial region of the jet and sharp-edged outlet. The width of the slot, B, is 5 mm. The longitudinal length of the slot is 25 mm, which is 5 times of width of slot. Thus, the pre-development of flow would occur through the slot passage.

In this study, particle image velocimetery (PIV) system, as shown in Fig. 6, was used to measure the velocity profiles and to identify the turbulent characteristics. The general procedure of using a PIV system is as follows (TSI, 1995). Tracer particles are added to the discharge flow. A light sheet from the laser system was used to illuminate the particles at least twice within a short time interval on a plane through the cen-

Table 1. Values of Parameters for Plane Jet Experiments

Case	Q(*l*/hr)	U(cm/s)	$Re_j(=UB/\nu)$	$F_i(=U/\sqrt{gB})$
NFJ100	100.0	5.56	278	0.251
NFJ150	150.0	8.33	417	0.376
NFJ200	199.0	11.06	553	0.499
NFJ200	249.0	13.83	692	0.625
NFJ300	293.0	16.28	814	0.735

terline of the jet. The light scattered by the particles is recorded either on a single frame or on a sequence of frames. The displacement of the particle image between the light pulses is determined through the evaluation of the PIV recordings. The sophisticated post-processing is required to handle the great amount of data collected through the employment of the PIV system.

3.2 Experimental Conditions

The slot was placed horizontally with the vertical distance of 43 cm from the tank bottom to the center of the chamber. The initial water depth were 86 cm for all cases. The temperature difference (< 1°C) between the ambient and jet fluid are negligible. The spacing of the measuring grid was 0.6 mm. In this study, the interested region was limited to $36B \times 18B$(18 cm × 9 cm) connecting two image planes to the longitudinal direction due to the limitation of laser system that does not provide equal laser intensity on the whole image plane. Therefore, the CCD camera and PIV laser installed on automatic traverse systems were moved horizontally and vertically.

Instantaneous velocity profiles were sampled at 15 Hz. This sampling rate (15 Hz) of the PIV system used in the measurement may not be enough to analyze the turbulent characteristics of the plane jet. However, this study focuses on the large-scale transition behavior rather than the fluctuation generated by small-scale turbulence. The time interval between two successive images was 500 μs. 330 instantaneous velocity profiles were collected since the instantaneous velocity profiles were sampled during 22 seconds The experimental conditions of typical cases conducted in this study are listed in Table 1.

4. EXPERIMENTAL RESULTS

4.1 Mean Velocity Profiles

Fig. 7 shows the velocity vector fields for NFJ300. The variables representing flow velocities are normalized by the nominal outlet velocity, U. In the figure, the potential core is observed near the initial region of the slot jet. Eq. (9) represents the potential core length, $x=5.21B$ In the figure, it is seen that the velocity fields tend to be Gaussian distribution after $x \cong 5B$. It is also noted that the jet width grows while the centerline velocity decreases with x/B. In the figure, the reverse flows occur outside of the jet boundary. It is expected that the wall effect resulting from the entrainment of ambient water into the jet region may lead to the reverse flow outside of the jet.

The Fig. 8 shows the lateral velocity distributions at different axial distances for several cases. From the figure, one can not find exact top-hap distribution of the velocity in potential core even though the potential core is observed near the initial region of the slot jet. It may be resulted

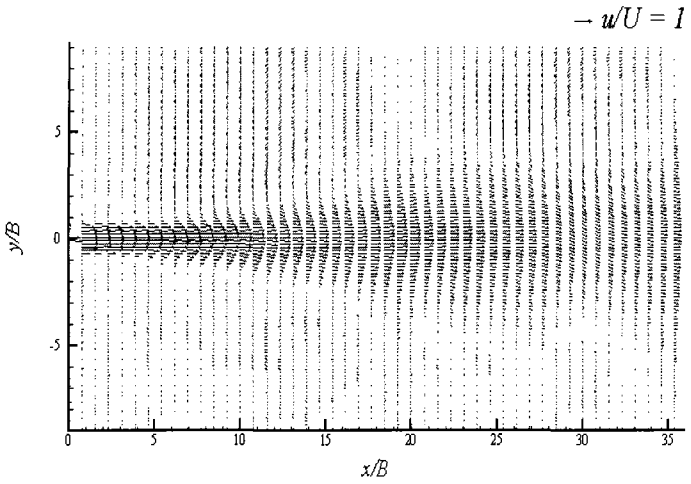

Fig. 7. Velocity Vector Fields for NFJ300

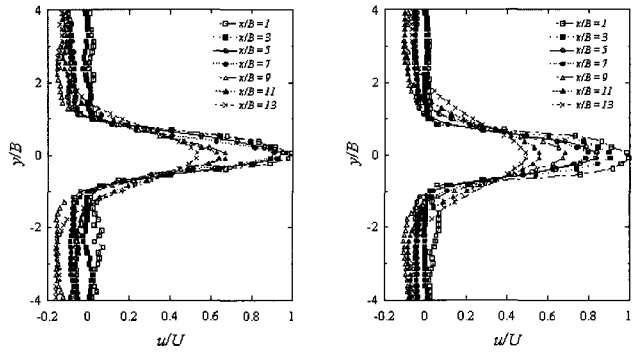

(a) NFJ150 (b) NFJ200

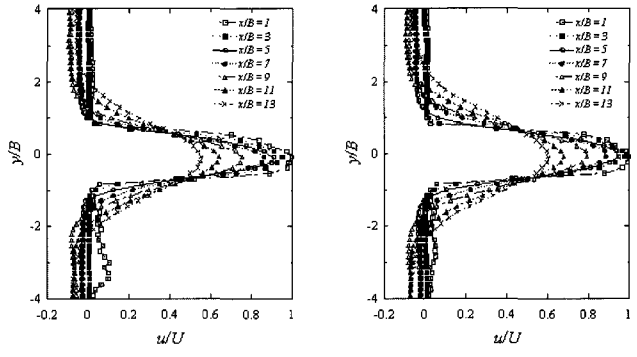

(c) NFJ250 (d) NFJ300

Fig. 8. Lateral Velocity Distribution

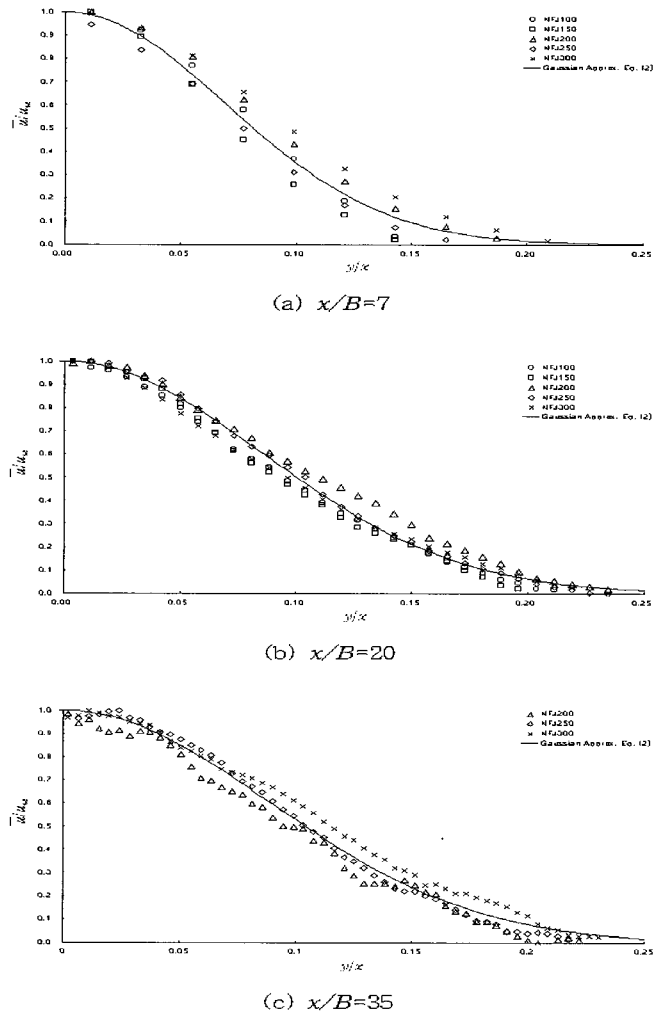

Fig. 9. Lateral Velocity Profiles for Non-Buoyant Jet

from the pre-development of the flow as mentioned previously. Fig. 8 shows the similar velocity profiles in each case. It is also clearly observed that the centerline velocity of each section decreases with increasing x/B.

Lateral velocity profiles at x/B=7, 20 and 35 are plotted in Fig. 9, respectively. It is considered that x/B = 7 and 20 are classified as the transition region whereas x/B = 35 is the self-preserving region. In this study, in order to check the similarity of velocity profiles (Kuang *et al.*, 2001), velocity profiles were fitted by Gaussian distributions, Eq. (2). The coefficients k_u in Eq. (2) found for various x/B are listed in Table 2. This table shows that k_u decreases with x/B in the transition region. The early experimental studies proposed that k_u is conserved in the self-similar region. Chen and Rodi (1980) found that ku is 57. In this study, the variation of k_u decreases gradually and reaches nearly

Table 2. Variation of k_u in the Selected Region

Distance form Inlet (x/B)	k_u	Region
7	105	transition region
20	69	transition region
26	66	transition region
34	64	self-similar region
35	64	self-similar region

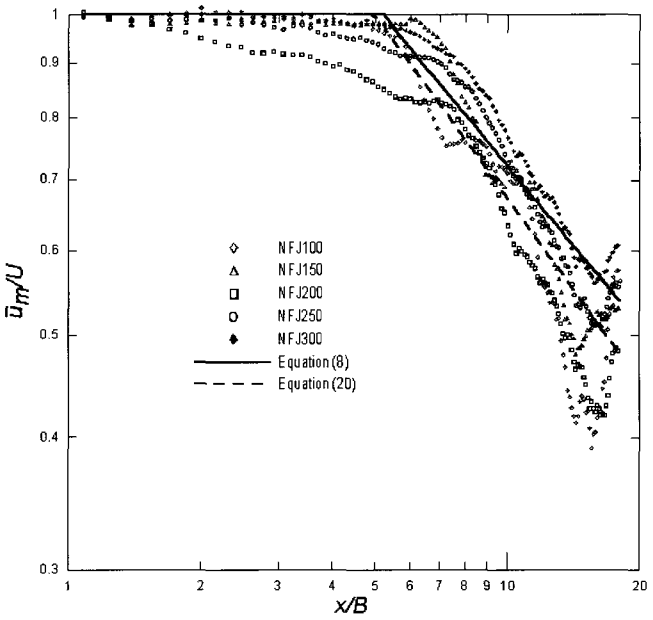

Fig. 10. Longitudinal Variation of Centerline Velocity for Non-Buoyant Free Jet

constant value of 64 on the range of x/B of 34 – 35 as seen in Table 2. This implies that the experimental coefficient of k_u = 64 reflects the self-similar region. I_2 is defined in Eq. (5). Substitution of the Gaussian distribution into Eq. (5) and integration give

$$I_2 = \sqrt{\frac{\pi}{2k_u}} \tag{18}$$

Thus, it is proposed that I_2 depends only on k_u.

The longitudinal variation of the centerline velocities is presented in Fig. 10. The centerline velocity decay is much slower in the ZFE region than that in the ZEF. A theoretical expression of the longitudinal distribution of centerline velocity, Eq. (8), is also plotted in Fig. 10. In this figure, the theoretical equation tends to overestimate the measured centerline velocity in the transition region. This is considered because Eq. (8) is derived using constant I_2 However, it is seen that I_2 depends on x/B in the transition region. Therefore, it should be considered that I_2 is a function of x/B

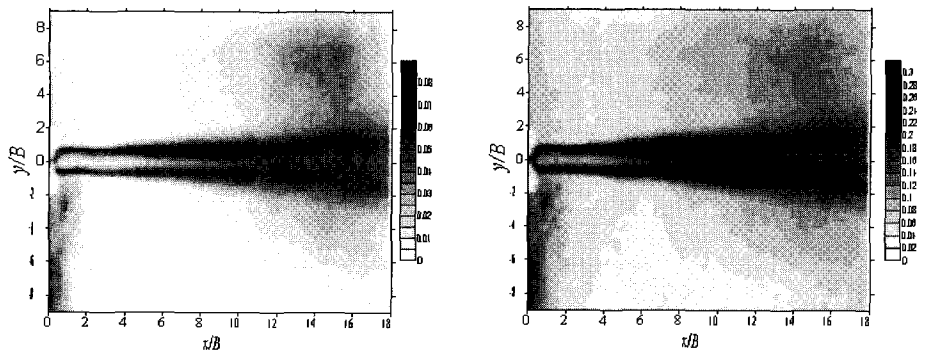

Fig. 11. Contours of Turbulent Characteristics for NFJ300
(a) k/U^2 **; (b)** $\sqrt{\overline{u'^2}}/U$

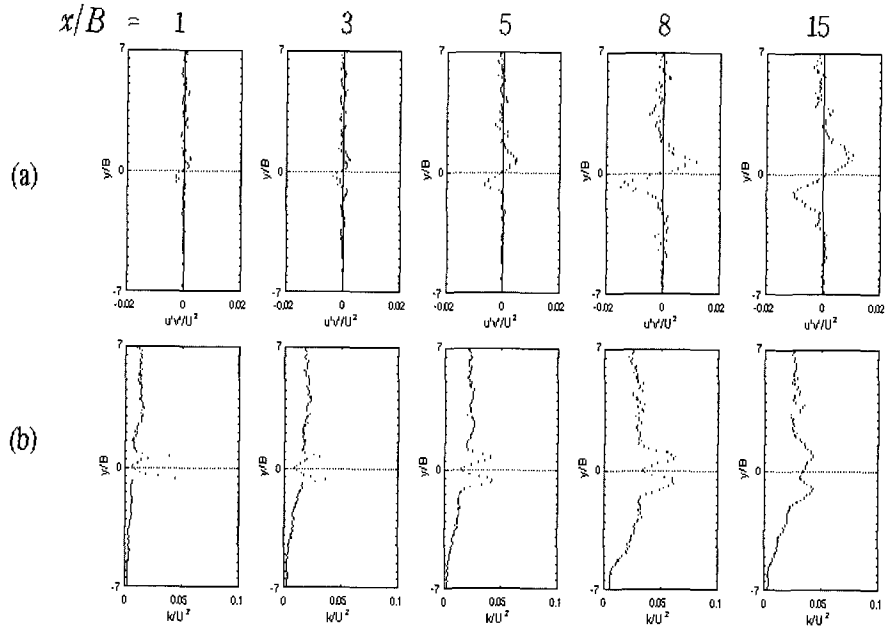

Fig. 12. Streamwise Development of Turbulent Characteristics for NFJ300
(a) $\overline{u'v'}/U^2$ **; (b)** k/U^2

($I_2 \propto (x/B)^{0.146}$). Substituting this relation into Eq. (6), the normalized centerline velocity can be derived as

$$\frac{\bar{u}_m}{U} = C\left(\frac{x}{B}\right)^{-0.573} \qquad (x > L_0) \tag{19}$$

where C is a constant. The constant, C, is closely related to the potential core length, L_0.

In this study, it is proposed that $L_0 = 5.0B$. Appling $\bar{u}_m / U = 1$ at $x = L_0$, the constant C is determined to be 2.515. Therefore, Eq. (19) becomes

$$\frac{\bar{u}_m}{U} = 2.515\left(\frac{x}{B}\right)^{-0.573} \quad (x/B > 5.0). \tag{20}$$

In Fig. 10, it is seen that the centerline velocity in the ZFE gradually and slightly decreases with the jet axis even if the centerline velocity in the potential core is theoretically undiminished as mentioned previously. This also implies that the pre-development of the flow inside the nozzle may result in the slight centerline velocity decay in the ZFE. In this Figure, it is observed that the proposed equation, Eq. (20), seems to be in better agreement with the measured data than Eq. (8) in the transition region.

4.2 Turbulent Characteristics

The turbulent kinetic energy, k, turbulent intensity ($\sqrt{\overline{u'^2}}$), and Reynolds shear stress have been used to describe the turbulent characteristics of the jet. In this study, these variables are normalized by nominal outlet velocity, U. Fig. 11 shows the contours of turbulent kinetic energy and turbulent intensity for the case of NFJ300. In this figure, turbulent kinetic energy k is defined as

$$k = 0.75(\overline{u'^2} + \overline{v'^2}) \tag{21}$$

where u' and v' are turbulent fluctuations in x and y directions, respectively. These figures show peak values are concentrated on the shear layers. The potential core and the center of the jet show the small turbulent motion. It is also noted that the potential core gets reduced as the turbulence penetrates to the jet axis.

Fig. 12 shows the streamwise profiles of the normalized Reynolds shear stress, and turbulent kinetic energy for the case of the NFJ300. In this figure, Reynolds shear stress is defined as

$$\tau = -\rho\overline{u'v'} \tag{22}$$

where ρ is fluid density.

The peaks of Reynolds shear stress and turbulent kinetic energy profile reflect the existence of the shear layers. The Reynolds shear stress profiles show the positive peak in the upper layer and negative peak in the lower layer. The profiles for the turbulent kinetic energy also provide the double peak features on these layers. In Fig. 12, it is noted that the peak of the Reynolds shear stress increases until x/B=8, and then it decreases afterwards. This phenomena is also observed in the turbulent kinetic energy profiles.

5. CONCLUSIONS

The laboratory experiments of non-buoyant plane jet were performed to obtain the mean velocity profiles and turbulent characteristics using PIV system. The rectangular nozzle used in this study has the aspect ratio of 20. The results of the theoretical equation based on the point source concept by Pani and Parameswaran (1994) show that the rectangular jet in the region of x/B<70 can be analyzed two-dimensionally at the center of nozzle.

The experimental results show that the lateral velocity profile is in good agreement with Gaussian distribution. However, the coefficient (k_u) of Gaussian distribution decreases with longitudinal distance in the transition region. Since the velocity profiles were fitted by Gaussian distributions, the coefficients k_u have been estimated to be 105, 69, 66 and 64 for x/B=7, 20, 26, and 35, respectively. In this study, it can be proposed

that the experimental coefficient of k_u = 64 reflects the self-similar region.

The existing theoretical equation for the centerline velocity tends to overestimate the measured data in the transition region. This is considered because the theoretical equation is derived using constant k_u. In this study, a new equation for the centerline velocity was proposed by consideration of k_u as a fuction of x/B. The centerline velocity based on this equation decays slightly faster than the previous theoretical equation using constant k_u. In the transition region, the proposed equation is in better agreement with the measured data than the previous theoretical equation.

The results of the turbulence characteristics show peak values are concentrated on the shear layers. The potential core and the center of the jet show the small turbulent motion. It is also noted that the potential core gets reduced as the turbulence penetrates to the jet axis. The Reynolds shear stress profile shows the positive peak in the upper layer and negative peak in the lower layer whereas the turbulent kinetic energy provides double peaks at the shear layers. The peak of the Reynolds shear stress and the turbulent kinetic energy increases until x/B=8, and then it decreases afterwards.

ACKNOWLEDGEMENTS

This research work was partially supported by the 1999-2000 Research Fund 1999-2-309-004-3 of the Korea Science and Engineering Foundation and the 2000-2001 Brain Korea project of the Ministry of Korea. This research work has been conducted in the Research Institute of Engineering Science of Seoul National University, Seoul, Korea.

REFERENCES

Albertson, M., Dai, Y. B., Jensen, R. A., and Rouse, H. (1950). "Diffusion of submerged jets." *Trans. ASCE*, 115, 639.

Chen, C. J. and Rodi, W. (1980). Vertical turbulent buoyant jets-a review of experimental data. *HTM series 4*. Perganon, Tarrytown, N.Y

Crow, S. C. and Champagne, F. H. (1971). "Orderly structure in jet turbulence." *Journal of Fluid Mechanics*, Vol. 48, Part 3 pp. 547-591.

Daily, J. W. and Harleman, D. R. F. (1966). *Fluid dynamics*, Addison-Wesley Publishing Company, Inc.

Fischer, B. H., List, E. J., and Koh, R. C. Y., Imberger, J., and Brooks, N. H. (1979). *Mixing in inland and coastal waters*. Academic Press, Inc., New York, N.Y.

Gutmark, E. J. and Grinstein, F. F. (1999). "Flow control with noncircular jets." *Annual Review of Fluid Mechanics*, Vol. 31, pp. 239-272.

Kim, Y., Seo, I. W., and Ahn, J. K. (2001). "Flow characteristics of a two-dimensional neutrally buoyant jet in a model settling tank." *Water Engineering Research*, Vol. 2, pp. 21-31.

Kuang, J., Hsu, S., and Qiu, H. (2001). "Experiments on vertical turbulent plane jets in water of finite depth." *Journal of Engineering Mechanics*, ASCE, Vol. 127, No. 1, pp. 18-26.

Lozanova, M. and Stankov, P. (1998). "Experimental investigation on the similarity of a 3D rectangular turbulent jet." *Experiments in Fluids*, Vol. 24, pp. 470-478.

Morton, B. R., Taylor, G. I., and Turner, J. S. (1956). "Turbulent gravitational convection from maintained and instantaneous sour-

ces." *Proc. Royal Society*, Vol. A234, pp. 1-23.

Pani, B. S. and Parameswaran, P. V. (1994). "Momentum and heat flux characteristics of three dimensional jets based on point-source concept." *Journal of Hydraulic Research*, Vol. 32, pp. 53-66.

Rajaratnam, N. (1976) *Turbulent jets*, Elsevier Scientific Publishing Company, Amsterdam

TSI (1995). *Particle image velocimetry (PIV): Theory of Operation.*

Il Won Seo, Prof., Dept. of Civil Engineering, Seoul National Univ., Seoul, Korea
(E-mail : seoilwon@plaza.snu.ac.kr)

Jung Kyu Ahn, Grad. Student, Dept. of Civil Engineering, Seoul National Univ., Seoul, Korea
(E-mail : ajk38317@orgio.net)

Seok Jae Kwon, Grad. Student, Dept. of Civil Engineering, Seoul National Univ., Seoul, Korea
(E-mail : sj79kwon@chollian.net)